Pergamon

Cement and Concrete Research 31 (2001) 343–349

CEMENT AND CONCRETE RESEARCH

# Galvanostatic testing for the durability of marine concrete under fatigue loading

W. Ahn[a,*], D.V. Reddy[b]

[a]BERGER/ABAM Engineers Inc., Marine Structures Division, Suite 300, 33301 Ninth Avenue, South, Federal Way, WA 98003-2600, USA
[b]Center for Marine Structures and Geotechnique, Department of Ocean Engineering, Florida Atlantic University, Boca Raton, FL, USA

Received 31 August 1998; accepted 14 December 2000

**Abstract**

Fatigue loading is a significant factor in determining the service life of the marine concrete structures, as it considerably enhances the deterioration process in a corrosive marine environment. To evaluate the durability of marine concrete structures subjected to fatigue loading, accelerated laboratory testing was carried out on full- and half-size reinforced concrete specimens, subjected to static and fatigue loading with three different water cement ratios (w/c = 0.3, 0.4, and 0.6). The marine tidal zone was simulated by alternate filling and draining of the tank, and a galvanostatic corrosion technique was used to accelerate corrosion of the reinforcement. Half-cell potential measurements and crack investigations were followed by ultimate strength testing. The significant findings include the adverse effect of fatigue loading, existence of an explicit size effect, and the negative effect of increasing water/cement ratio. 

*Keywords:* Acceleration; Corrosion; Durability; Fatigue

## 1. Introduction

Concrete is widely used in nearshore and offshore marine structures, bridge substructures, and superstructures. Experience has shown that the durability of marine concrete structures is generally good. This is not to say that the experience has been undividedly satisfactory, as long as numerous structures with poor performance can be found in the coastal areas [1]. The lack of durability can very often be attributed to factors such as mixture design, cover depth, exposure conditions, structural design details, maintenance routines, etc. There are still many unexplained factors in the deterioration process and the relation between the deterioration and the durability of marine concrete structures. This is because of the uncertainties in the construction process and environmental conditions affecting the deterioration of reinforced concrete. Once concrete is placed in the sea, maintenance becomes very difficult and expensive due to its surrounding environment [2].

The magnitude of the durability problem is considerable enough to merit national action. It is easily deduced that the most aggressive exposure a marine concrete can routinely experience is in the tidal zone [3]. Lack of durability is manifested in the form of cracking, spalling, loss of strength, or loss of mass. Concrete in an advanced state of deterioration is generally found to be suffering from more than one cause, and it usually becomes very difficult to identify the first cause which might have broken down the ability of concrete to resist attack from a host of other causes. The damage to concrete structures, resulting from the corrosion of reinforcing steel, is exhibited in the form of expansion, cracking, and spalling of concrete cover. In addition to the cover loss, a reinforced concrete member may suffer structural failure due to loss of bond between concrete and steel. This is why the corrosion of reinforcing steel is considered to be the most serious problem responsible for lack of durability [4]. Many marine concrete structures, such as floating structures, mobile drilling structures, offshore structures, and bridges, are subjected to a number of fatigue cycles. Fatigue loading is a significant factor in determining the life of the structure, besides corrosion, as it considerably enhances the deterioration process in a corrosive marine

* Corresponding author. Tel.: +1-206-431-2300; fax: +1-206-431-2250.
*E-mail address*: ahn@abam.com (W. Ahn).

0008-8846/01/$ – see front matter 
PII: S0008-8846(00)00506-8

Table 1
Details of specimens

| Cement | ASTM C150 Type II |
|---|---|
| Water/cement ratio and 28 day compressive strengths | w/c = 0.3, 0.4, and 0.56<br>$f_c'$ = 68.4, 52.4, and 31.4 MPa, (9918, 7598, and 4553 psi) |
| Specimen sizes | Full-size (0.3 × 0.3 × 2.36 m)<br>Half-size (0.15 × 0.15 × 1.18 m) |
| Steel | ASTM A616 Grade 60 |
| Coarse aggregate | Max. 9.53 mm (3/8 in.) Florida Pearock |
| Slump | 76–102 mm (3–4 in.) |
| Air content | 4 ± 1.5% |
| Admixtures | Air entrainer and water reducing agent |
| Total number of beam specimens = 16 | |
| 8 full-size beams: FS3, FD3, FS4, FD4, FS4, FD4, FD3, FS3 | |
| 8 half-size beams: HS4, HD4, HS6, HD6, HD4, HD6, HS4, HS6 | |
| Legend for notation | |
| 1st character: specimen size (F for full-size, H for half-size) | |
| 2nd character: load condition (S for static, D for dynamic) | |
| 3rd character: water–cement ratio (3 for 0.3, 4 for 0.4, and 6 for 0.56) | |

environment. The increased cracking due to fatigue loading heads to easier chloride penetration.

## 2. Objectives

The objectives of this study were as follows: (1) to evaluate whether specimens subjected to fatigue loading behave differently from those subjected to static loading, (2) to evaluate the deterioration characteristics of specimens with different w/c (water/cement ratios), and to evaluate the size effect between full- and half-size specimens.

## 3. Experimental investigation

### 3.1. Methods and materials

A total of 16 concrete beams was used for the testing with different water/cement ratios (0.3, 0.4, and 0.6), sizes (full and half), and loading conditions (fatigue and static). Table 1 shows the details of specimens. The dimensions of the specimens (lengths, widths, depths, cover thickness, and rebar sizes) were determined by an iteration method. By changing the variables, i.e. reinforcement size, beam depth, and cover thickness, iteration was carried out until the same stresses due to bending were applied to the cross sections of the beams and bottom reinforcement of the full- and half-size specimens, with load levels (third-point loading), P for full-size, and P/4 for half-size specimens. The method of stress calculation was based on ACI 318-99, 10.3.1. Fig. 1 shows the dimensions of full- and half-size specimens.

### 3.2. Fatigue and static loading testing

The tests were carried out on eight full-size 12 × 12 × 93 in. (0.3 × 0.3 × 2.36 m) and eight half-size 6 × 6 × 46.5 in. (0.15 × 0.15 × 1.18 m) concrete beam specimens with three different w/c ratios (0.3, 0.4, and 0.56) at the Ocean Front

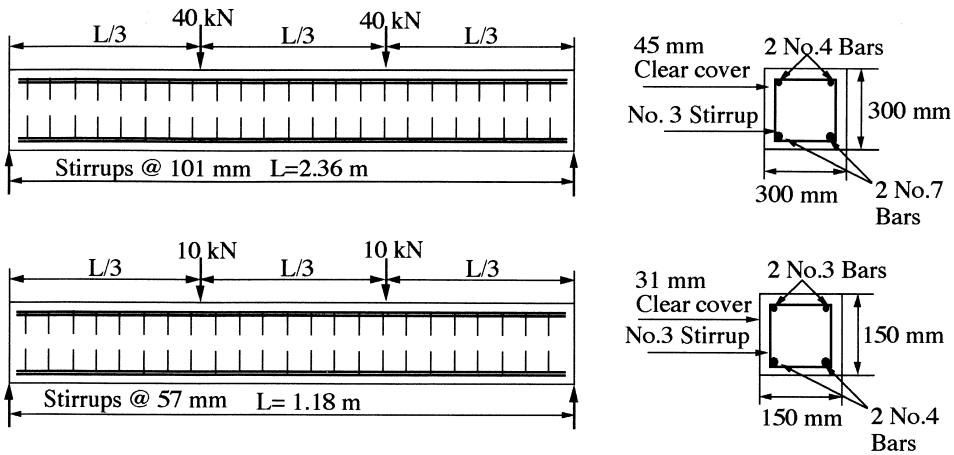


Fig. 1. Details of full- and half-size specimen.

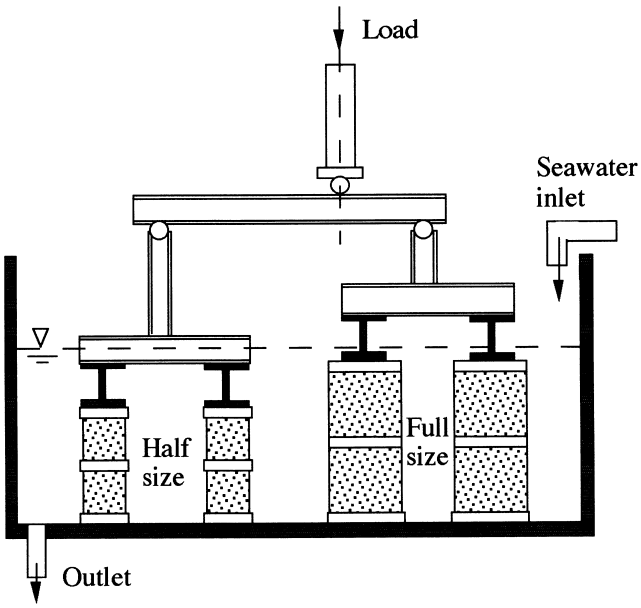


Fig. 2. Transverse section of fatigue test set-up.

Laboratory. One set of four full-size and another set of four half-size concrete beams were subjected to four-point fatigue loading with 0.01 Hz frequency (Figs. 2 and 3). Two companion sets of four full- and four half-size concrete beams were subjected to four-point static loading in yoked setups (Fig. 4). The details of the specimens are shown in Table 1. The load levels were selected to cause initial cracks, with smaller crack widths than the maximum permissible crack width, 0.006 in. (0.15 mm) for marine concrete [5]. The 45 kips (200 kN) maximum fatigue load [minimum load = 5 kips (22.2 kN)] from the actuator was distributed as

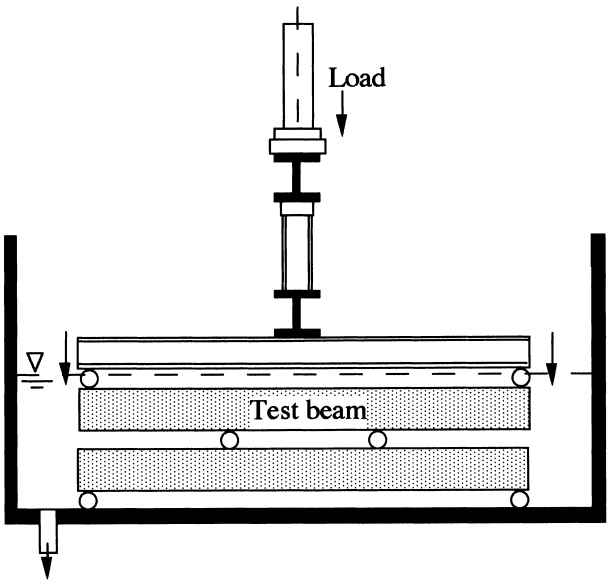


Fig. 3. Longitudinal elevation of fatigue test setup.

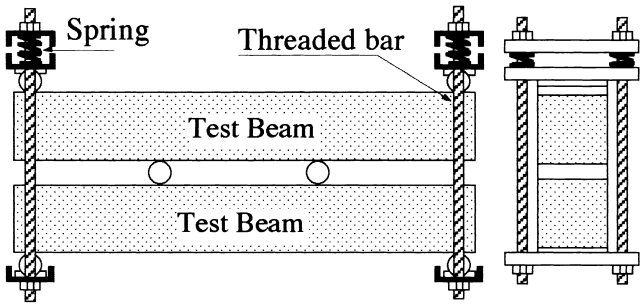


Fig. 4. Control beams under static loading.

18 kips (80 kN) for each full-size specimen and 4.5 kips (20 kN) for each half-size specimen by the load distribution setup. Spring forces were applied to the control beams as static loading, 18 kips (80 kN) and 4.5 kips (20 kN) for each of the full- and half-size specimens, respectively, by tightening the nuts on the sandwich yoked setup (Fig. 4). All beam specimens were exposed to simulated tidal conditions by alternate filling and draining of natural seawater in the tank every 12 h.

### 3.3. Corrosion acceleration by the galvanostatic technique

The galvanostatic technique was used to accelerate reinforcement corrosion by impressing anodic direct current. Each set of beams was connected in series with the constant current flowing through all the beams. Stainless steel 303 bars were used for the counter electrodes; the two bars were mounted in parallel near the concrete tension surfaces in the maximum bending moment region (Fig. 5). Current levels applied during the wet cycle were changed to observe the change of behavior of the beams at different current levels. These current levels were as follows: (1) For the first 30 days: no current, and (2) from 30 to 60 days: 190 mA (current density = 1.721 A/m$^2$) and 24 mA (0.761 A/m$^2$) on each of the full- and half-size specimens. (3) From the 60th day to the end of the exposure: 380 mA (3.442 A/m$^2$) and 48 mA (1.522 A/m$^2$) for each of the full- and half-size specimens. The current levels to induce measurable corro-

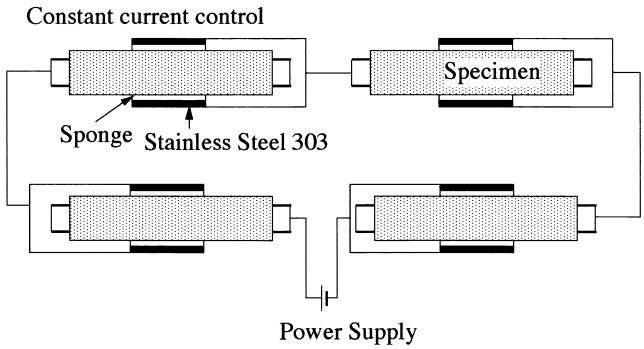


Fig. 5. Arrangement of galvanostatic corrosion.

sion were determined by using Faraday's law and the flexure formula for concrete beams, taking into consideration the reduced cross-sectional area of bottom tensile reinforcement after corrosion.

## 4. Test results

### *4.1. Half-cell potential readings during the exposure*

Half-cell potentials were measured periodically on all the beam specimens with a saturated calomel electrode (SCE) during the last 1 h of the dry cycle (right before the wet cycle), while specimens were not anodically polarized for the measurement. Preliminary measurements showed that it took about 9 h for the FS3 beam and about 3 h for the HS4 beam to eliminate the anodic polarization, after the constant anodic current supply was cut off automatically during the dry cycle. Measurements were carried out according to ASTM C876-87 from the beginning of the exposure at an interval of at most 10 days. Table 2 shows the half-cell potential readings during the exposure.

It was difficult to determine the corrosion tendency of the reinforcement in the seawater environment by employing the standard test method for half-cell potential measurement described in ASTM C876 (for atmospheric environment). This is because potential measurements indicate only the local probability of corrosion and not the actual corrosion rates. According to the ASTM standard, there is a greater than 95% probability that the reinforcing steel is corroding at the measured potential values (versus SCE) more negative than $-273$ mV. However, the measured half-cell potentials could be used for comparison of the active corrosion tendency of the various types of specimens under different loading conditions.

The periodic half-cell potentials for the specimens subjected to fatigue loading were different from the statically loaded ones. Some specimens under fatigue loading had more positive half-cell potentials than those under static loading for the first month of the exposure. With further exposure, the values for those under fatigue loading became more negative until the end of the exposure period (90th day of exposure). Fig. 6 shows a comparison of change of half-cell potentials for different loading conditions. Therefore, an adverse effect of fatigue loading on half-cell potential could be noticed. Full-size specimens with w/c = 0.3 showed more positive values than those with w/c = 0.4; and half-size specimens with w/c = 0.4 had more positive values than those with w/c = 0.6. It could be inferred that the reinforcement in concrete with higher w/c ratios had the more active corrosion tendency compared to those with lower w/c ratios.

Table 2
Periodic half-cell potential readings (mV, SCE)

| Day | FD3 | FS3 | FD4 | FS4 | HD4 | HS4 | HD6 | HS6 |
|---|---|---|---|---|---|---|---|---|
| 1 | −64 | −183 | −108 | −157 | −31 | −56 | −12 | −64 |
| 10 | −349 | −426 | −305 | −352 | −333 | −370 | −505 | −558 |
| 30 | −360 | −433 | −440 | −392 | −347 | −352 | −587 | −548 |
| 46 | −458 | −434 | −486 | −472 | −505 | −467 | −628 | −582 |
| 65 | −480 | −424 | −492 | −452 | −527 | −457 | −618 | −544 |
| 78 | −492 | −428 | −519 | −467 | −532 | −463 | −603 | −566 |
| 90 | −510 | −439 | −528 | −480 | −549 | −478 | −638 | −578 |

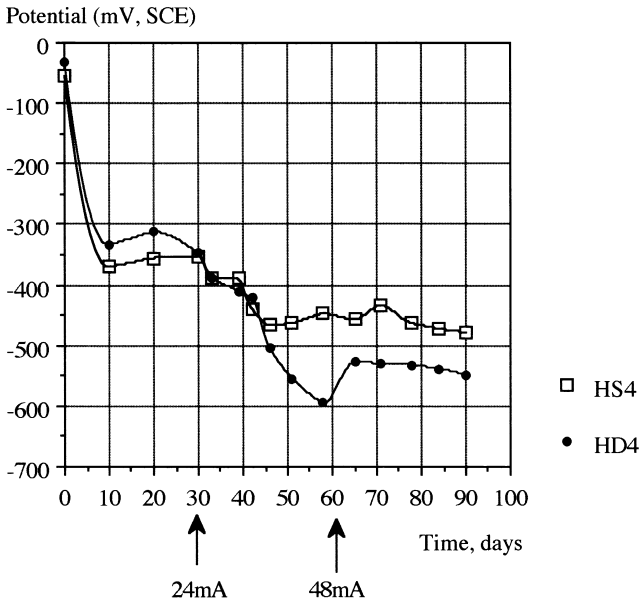


Fig. 6. Half-cell potentials for HD4 and HS4.

### *4.2. Final half-cell potential measurements*

After 78,000 fatigue cycles with simulated tidal exposure, the beams were dried in air for at least 10 days, and the half-cell potentials at different locations along the rebar were measured. All of them showed more negative potentials in the maximum bending moment region than near the ends. Also, the negative potentials were larger in the reinforcement on the tension side than that those on the compression side reinforcement. The measured potentials on the tension side in the maximum bending moment region from all the beams were considerably more negative than the value, $-273$ mV, SCE, that has been proposed by the ASTM standard C876 for 95% likelihood of corrosion. Therefore, reinforcement located on the tension side in the maximum bending moment region had more active corrosion tendency compared to that in the other regions. Furthermore, more negative potentials were noticed near the cracks with rust staining in many cases. Even though the readings did not give any information on the extent and rate of corrosion on reinforcement, they indicated that the reinforcement located near cracks has a larger probability for active corrosion than that further away from the cracks.

Beams subjected to fatigue loading showed more negative potentials than those with static loading in the maximum bending moment region. It was also found that the

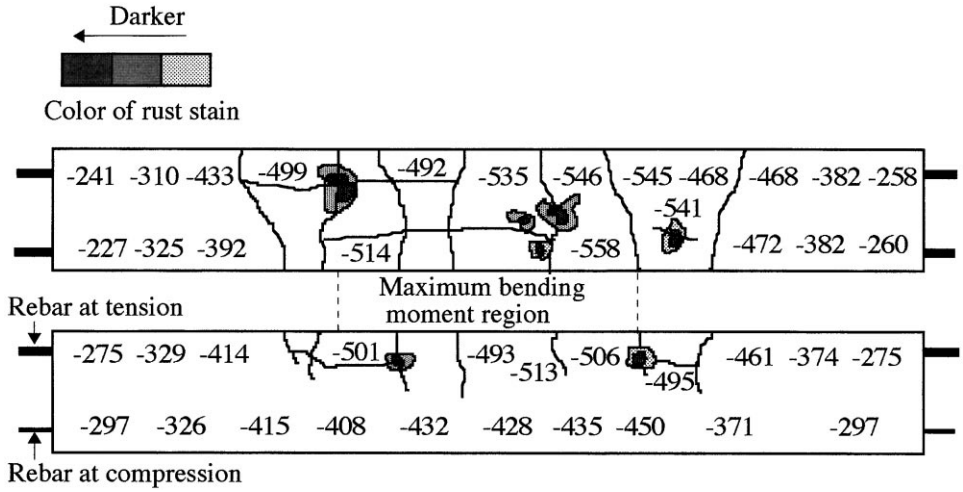


Fig. 7. Final half-cell potentials (mV, SCE) and cracks on FD4.

potentials increased negatively as the w/c increased. Therefore, half-cell potential readings enabled the comparison of the corrosion tendency of beams subjected to different loading conditions with varying water/cement ratios. Fig. 7 shows the cracks, rust staining, and half cell potentials on the beams, FD4.

### 4.3. Crack investigation

Crack shapes of all the beams were observed after the exposure testing. Most of the beams showed more rust staining in the middle maximum moment region, indicating more corrosion damage than in the other regions (Fig. 7). The longitudinal cracks observed propagated from transverse cracks and sometimes bridged two or more transverse cracks (Fig. 7). Based on the larger negative half-cell potentials measured, the corrosion damage on the main reinforcement, close to transverse cracks, was more severe than that further away from the cracks. On the other hand, transverse cracking resulted not only from loading, but also from corrosion-induced damage of stirrups. The similarity of the cracks formed by galvanostatic corrosion to those formed during the long-term exposure test by Kobayashi and Hoshino (referenced by Uomoto and Misra [6]), indicates the adequacy of the galvanostatic method to accelerate the corrosion process in the laboratory tests. Therefore, an interaction between the effects of corrosion and loading is identified for the deterioration of marine concrete in the simulated laboratory investigation.

Table 3
Nominal strength, average ultimate strength, and strength comparison factor

| Beams | FS3 | FD3 | FS4 | FD4 | HS4 | HD4 | HS6 | HD6 |
|---|---|---|---|---|---|---|---|---|
| Nominal strength, $f_n$ (MPa) | 29.1 | 29.1 | 28.9 | 28.9 | 28.9 | 28.9 | 27.7 | 27.7 |
| Ultimate strength, $f_u$ (MPa) | 25.1 | 23.7 | 23.6 | 22.5 | 31.4 | 29.7 | 28.8 | 28.1 |
| Strength comparison factor, $R$ | 0.86 | 0.82 | 0.81 | 0.78 | 1.08 | 1.03 | 1.04 | 1.02 |

### 4.4. Ultimate strength

After 78,000 fatigue cycles, ultimate strength testing was carried out by applying four-point flexural loading. The failure mode observed from all the beams at ultimate strength was a flexural failure, enhanced by longitudinal cracking due to corrosion on reinforcement on tension side. The ultimate and nominal strength values of the beams are compared in Table 3. The relative degree of deterioration can be expressed by the strength comparison factor, $R$, which can be calculated as follows [Eq. (1)]:

$$R = f_u/f_n, \tag{1}$$

where $f_n$ is the nominal strength of nondeteriorated beams calculated from the formula (ACI 318-99 Building Code 10.3.1), and $f_u$ is the ultimate strength from the test results.

The findings are as follows: (1) Ultimate strengths of all the half-size beams were higher than those for the full-size ones. (2) Beams subjected to fatigue loading during the exposure period showed lower ultimate strengths than those subjected to static loading, both full- and half-size. (3) The ultimate strengths decreased with increasing w/c.

### 4.5. Size effect of the deteriorated reinforced concrete

The ultimate strength test results showed explicit evidence of the size effect for two deteriorated beams geometrically similar to each other. The Bazant size effect model

Table 4
Size effect models on ultimate strength at the failure for different concrete mixtures and loading conditions during the exposure

| | Bazant's model | |
|---|---|---|
| Concrete mix | $f_u = B \times f_r[1 + d/(\lambda_o \times d_a)]^{-1/2}$ | $f_r$ (kPa) |
| S4 | $11.08\, f_r[1 + d/(7.25\, d_a)]^{-1/2}$ | 4505 |
| D4 | $9.88\, f_r[1 + d/(9.88\, d_a)]^{-1/2}$ | 4505 |

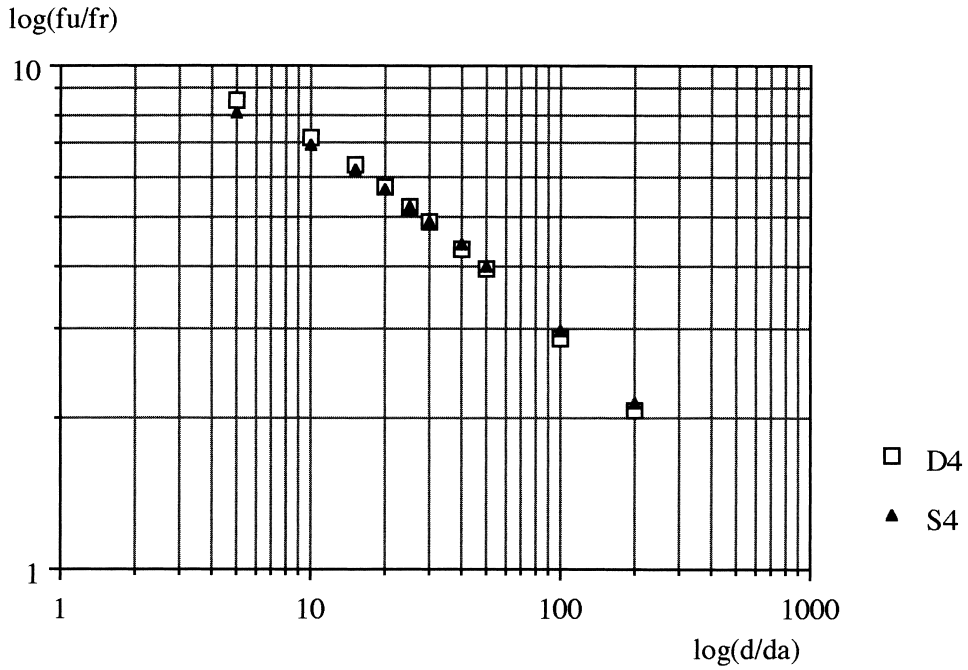


Fig. 8. General trend illustrating the effect of the ratio of beam depth to maximum size of coarse aggregate on ultimate strength.

[7] enables the evaluation of the test results and predicts the strengths of geometrically similar shape specimens with different aggregate sizes. Eq. (2) gives the size effect as follows:

$$f_u = \frac{Bf_r}{\sqrt{1+N}}, \tag{2}$$

where: $f_u$ = ultimate strength of the beam specimen; $f_r$ = modulus of rupture = $7.5\sqrt{f_c'}$, (ACI 318-99-9.5. 2.3); $f_c'$ = compressive strength of cylindrical specimen; $N = d/(\lambda_o d_a)$, the brittleness number; $d_a$ = the maximum size of coarse aggregate in the specimen = 9.5 mm; $d$ = size of the specimen, the depth of beam for this application; $B$ and $\lambda_o$ = empirical constants.

Empirical constants $B$ and $\lambda_o$ were determined from the ultimate strength test results for w/c = 0.4 full- and half-size specimens, (Table 4). The size effect models for two different loading conditions in Table 4 were plotted in Fig. 8 for different $d/d_a$ values. Fig. 8 shows that the general influences of the specimen and maximum coarse aggregate sizes are similar for all the four different expressions.

## 5. Conclusions

(1) The galvanostatic simulated laboratory investigation enabled the comparative evaluation of the interaction between the effects of corrosion and loading for the deterioration process of marine concrete.

(2) Beams deteriorated more rapidly under fatigue loading than static loading. They showed more and longer longitudinal cracks induced by corrosion at the end of the simulated marine exposure, and less ultimate strength bearing capacity, than those under static loading.

(3) The durability of reinforced concrete decreased with increasing water/cement ratios in a marine environment. Beams made with higher w/c mixtures had more negative half-cell potentials, less cracking resistance, and less ultimate strength bearing capacity. The utilization of dense and less permeable high-strength concrete with low w/c ratio can contribute to the enhancement of the durability of marine concrete structures.

(4) The major cracking patterns from accelerated testing (by galvanostatic method) were representative of those observed under long-term exposure of marine concrete structures, showing both transverse and longitudinal cracks along the beams.

(5) The size effect (a function of the ratio of the beam depth to maximum size of coarse aggregate) needs to be definitely considered in extrapolating the laboratory test results of concrete specimens to prototypes. This will avoid overestimation of prototype-strength based on laboratory testing.

## Acknowledgments

This paper is based on a National Science Foundation (NSF) funded project, "Experimental and Analytical Investigation of the Durability of Reinforced and Post-Tensioned Concrete in a Simulated Marine Environment" (Grant No. MSS-9105194). Thanks are due to the NSF

Contract Monitor, Dr. J.B. Scalzi, Program Director, Large Structural and Building Systems for his support and continued interest during the investigation. Appreciation is expressed to Dr. W.H. Hartt, Professor and Director of Center for Marine Materials, Department of Ocean Engineering, Florida Atlantic University for his valuable input.

## References

[1] B. Espelid, N. Nilsen, A field study of the corrosion behavior on dynamically loaded marine concrete structures, Concrete in Marine Environment Proceedings, Second International Conference, St. Andrews by the Sea Canada, ACI SP-109. American Concrete Institute, Detroit (Editor: V.M. Malhotra) 1988, pp. 85–104.

[2] D.V. Reddy, W. Ahn, Durability testing of marine reinforced concrete in a simulated marine environment, Proc. of the 20th Conference on Our World in Concrete and Structures, Singapore, CI-PREMIER PTE LTD, Singapore (Editor: C.T. Tam) August 23–25.

[3] P.K. Mehta, Durability of concrete in marine environment — a review, Performance of Concrete in Marine Environment, ACI SP-65, American Concrete Institute, Detroit (Editor: P.K. Mehta) 1980, pp. 1–20.

[4] P.K. Mehta, Durability of concrete — fifty years of progress, Proceedings of Second International Conference, Montreal Canada, ACI SP-126 vol. 1, American Concrete Institute, Detroit (Editor: V.M. Malhotra) 1991, pp. 1–31.

[5] ACI Committee 224, Control of cracking in concrete structures, J. Am. Concr. Inst., Proc. vol. 77 (1980) 3–20 (American Concrete Institute, October).

[6] T. Uomoto, S. Misra, Behavior of concrete beams and columns in marine environment when corrosion of reinforcing bars take place, Concrete in Marine Environment Proceedings of Second International Conference, St. Andrews by the Sea Canada, ACI SP-109. American Concrete Institute, Detroit (Editor: V.M. Malhotra) 1988, pp. 127–146.

[7] Z.P. Bazant, K. Xu, Size effect in fatigue of concrete, ACI Mater. J. 88 (4) (1991) 390–399 (July–August).